Integral Sliding-Mode Direct Torque Control of Doubly-Fed Induction Generators Under Unbalanced Grid Voltage

Si Zhe Chen, Norbert C. Cheung, *Senior Member, IEEE*, Ka Chung Wong, and Jie Wu

***Abstract*—An integral sliding-mode direct torque control (ISM-DTC) scheme with space-vector modulation for wind-energy conversion systems based on doubly-fed induction generators (DFIGs) under unbalanced grid voltage is proposed. The torque and power pulsations at twice the grid frequency caused by unbalanced grid voltage can be minimized by the proposed ISM-DTC scheme. Compared with existing control schemes of DFIGs under unbalanced grid voltage, the parametric uncertainties are included into the design procedure of sliding-mode controller, which guarantees the robustness of the controller. Because the torque and reactive power are directly controlled by the rotor voltage, the measurement, coordinate transformation, and symmetrical component extraction of rotor current are eliminated, which simplifies the structure of the controller. Simulation and hardware implementation results validate the effect and parametric robustness of the proposed ISM-DTC scheme.**

***Index Terms*—Direct torque control (DTC), doubly-fed induction generator (DFIG), integral sliding-mode control, unbalanced grid voltage, wind-energy generation.**

NOMENCLATURE

F	Variable representing voltage, current and flux.
i_s, i_r	Stator and rotor winding current.
L_m	Magnetizing inductance.
L_s, L_r	Stator and rotor self-inductance.
L_{ls}, L_{lr}	Stator and rotor leakage inductance.
p_n	Number of pole pairs.
P_s, Q_s	Stator active and reactive power.
R_s, R_r	Stator and rotor winding resistance.
T_e	Electromagnetic torque.
u_s, u_r	Stator and rotor winding voltage.
φ_+, φ_-	Phase shift for positive- and negative-sequence components.
λ_s, λ_r	Stator and rotor flux.
ω_e, ω_r, $\omega_{\rm slip}$	Synchronous, rotor, and slip speed.
θ_e, θ_r, $\theta_{\rm slip}$	Angle of stator flux, rotor, and slip.
Δ	Parameter deviation.
Superscripts	
$+$, $-$	Positive- and negative-sequence synchronous reference frames.
$*$	Reference value for controller.
$\hat{}$	Conjugate complex.
Subscripts	
$+$, $-$	Positive- and negative-sequence components.
α, β	Stationary α–β axis.
d, q	Synchronous *d*–*q* axis.
s, r	Stator and rotor.
max, min	Upper and lower limits of the parameter.
0	Nominal value of parameter.

Manuscript received June 1, 2009; revised September 15, 2009; accepted October 30, 2009. Date of publication December 15, 2009; date of current version May 21, 2010. This work was supported in part by the National Natural Science Foundation of China under Grant 60534040 and the National High Technology Research and Development of China under Project 863 Program 2007AA05Z244. The work of S. Z. Chen was supported by the Hong Kong Polytechnic University under Grant G-U497. Paper no. TEC-00218-2009.

S. Z. Chen and J. Wu are with the College of Electric Power, South China University of Technology, Guangzhou 510640, China (e-mail: cszscut@126.com; epjiewu@scut.edu.cn).

N. C. Cheung and K. C. Wong are with the Department of Electrical Engineering, The Hong Kong Polytechnic University, Kowloon, Hong Kong (e-mail: norbert.cheung@polyu.edu.hk; eekcwong@polyu.edu.hk).

Digital Object Identifier 10.1109/TEC.2009.2036249

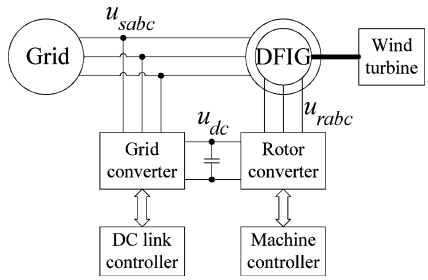

Fig. 1. WECS based on DFIG.

I. INTRODUCTION

THE mainstream high-power wind-energy conversion systems (WECSs) are based on doubly-fed induction generators (DFIGs). The stator windings of DFIGs are directly connected to the grids, and rotor windings are connected to the grids through back-to-back power electronic converters (see Fig. 1). WECSs based on DFIG offer several advantages over constant-speed WECSs, including maximizing power capture, reducing mechanical stresses, improving power qualities, and increasing transient stability margins of the electrical grids [1]. Comparing with synchronous generators, DFIGs are more suitable for high-power applications, because only a portion of the generated energy has to be processed by the power electronic converters [2].

WECSs are usually located in rural areas with weak grid connection, in which grid-voltage unbalance may arise even during normal operation. The grid-voltage unbalance may be caused by unbalanced transmission line impedance, unbalanced load, and large single-phase load. If the grid-voltage unbalance is not taken into account in the controller design, even a small

unbalanced grid voltage could introduce a highly unbalanced stator current, which will cause torque and power pulsations at twice the grid frequency. The torque pulsations will result in acoustic noise at low level and damage the rotor shafts, gearboxes, and blades at high level [3].

Various schemes based on vector control to eliminate torque and power oscillations of DFIGs under unbalanced grid voltage are proposed in [4]–[7]. Brekken and Mohan [4] extract the torque pulsations at twice the grid frequency, and then generates rotor-compensating voltage to compensate for the torque pulsations. Hence, the parameters of controller have to be carefully tuned to provide adequate gain for both the dc component and the double-frequency component in the synchronous reference frame. Xu and Wang [5] investigate the impact of unbalanced grid voltage on the torque and power pulsations, and proposes a dual-current controller to control the rotor positive- and negative-sequence currents in the positive- and negative-sequence synchronous reference frames, respectively. Hu *et al*. [6] propose an improved current-control scheme based on a proportional–integral (PI) plus resonant-current regulator in the positive-sequence synchronous reference frame and eliminates the decomposition of the rotor current into sequence components. The rotor-side convertor is controlled to limit the torque pulsation, and the grid-side convertor is controlled to limit the dc voltage ripples under unbalanced grid voltage in [7]. Two methods to separate positive- and negative-sequences components are also introduced and compared.

PI-based vector control is a popular and practical control method, which is proven effective by many researchers and industrial applications. In the control scheme, the nonlinear cross-coupling is eliminated with feed-forward compensation. With the compensation, the motor model becomes linear and PI control techniques can be applied. However, since the decoupling procedure involves motor parameters, the resulting control scheme is sensitive to these parameters [8]. Hence, the performance of vector control depends on the accuracy of motor parameters [9].

In practice, motor parameters are generally obtained by identification experiments in which errors are unavoidable. The parameters will also be influenced by the environment and operating condition, for example, the resistance may vary with temperature and the inductance may vary with magnetic saturation.

Because of the parameter dependence of vector control, direct power control (DPC) [9] and direct torque control (DTC) [10] have been proposed as alternatives to vector control. Santos-Martin *et al*. [11] propose a DPC scheme to achieve good dynamic responses and control power or torque oscillations under unbalanced voltage. The DPC scheme directly controls the power by selecting voltage vectors from a lookup-table according to the logic outputs of hysteresis controllers. However, the hysteresis control has some disadvantages, such as variable switching frequencies and current distortions, which will degrade the qualities of output power [10], [12].

In order to solve the parametric robustness issue of vector control and power quality issue caused by variable switching frequency in DPC or DTC, this paper proposes an integral sliding-mode DTC (ISM-DTC) scheme with space-vector modulation (SVM) to control DFIGs under unbalanced grid voltage.

The essential idea of sliding-mode control (SMC) is to enforce sliding-mode in a predefined sliding surface of the system state space. Once the state of system reaches the sliding surface, the structure of the controller is adaptively changed to slide the state of system along the sliding surface. Hence, the system response depends only on the predefined sliding surface and is insensitive to variations of system parameters and external disturbances. Interest in this control approach has emerged due to its potential to eliminate the effects of parameter variations with minimum complexity of implementation [8]. In recent years, a lot of research effort has been devoted to the application of SMC techniques to electrical drives and wind-energy generation [13]–[15].

Simulation and hardware experiment results are reported to validate that the proposed ISM-DTC scheme can effectively suppress ripples in torque and power. The experiment results of the unbalanced control method proposed in [5], in which two PI current controllers are used to control the rotor positive- and negative-sequence currents respectively, are obtained on the same platform for comparison. The results show that the proposed ISM-DTC scheme has better parametric robustness.

II. DFIG Model Under Unbalanced Grid Voltage

Based on symmetrical component theory, all unbalanced voltage, current, and flux vectors in the stationary reference frame can be represented as the superposition of positive-, negative-, and zero-sequence components. Since the neutral points of DFIGs are not connected to grids, all the zero sequence components are inexistent. Hence, in the stationary reference frame, the unbalanced voltage, current, and flux vectors can be decomposed into positive- and negative-sequence components as

$$\begin{aligned}\vec{F}_{\alpha\beta}(t) &= \vec{F}_{\alpha\beta+}(t) + \vec{F}_{\alpha\beta-}(t) \\ &= |\vec{F}_{\alpha\beta+}|e^{j(\omega_e t+\varphi_+)} + |\vec{F}_{\alpha\beta-}|e^{j(-\omega_e t+\varphi_-)}. \quad (1)\end{aligned}$$

The positive-sequence synchronous reference frame rotates at synchronous speed, while the negative-sequence synchronous reference frame rotates at the same speed but contrary direction. The transformations of variables among the stationary, positive-sequence synchronous and negative-sequence synchronous reference frame are given as

$$\begin{aligned}\vec{F}^{+}_{dq} &= \vec{F}_{\alpha\beta}e^{-j(\omega_e t+\varphi_+)} \qquad \vec{F}^{+}_{dq} = \vec{F}^{-}_{dq}e^{-j2\omega_e t}e^{-j(\varphi_+-\varphi_-)} \\ \vec{F}^{-}_{dq} &= \vec{F}_{\alpha\beta}e^{-j(-\omega_e t+\varphi_-)} \qquad \vec{F}^{-}_{dq} = \vec{F}^{+}_{dq}e^{j2\omega_e t}e^{j(\varphi_+-\varphi_-)}. \quad (2)\end{aligned}$$

All the unbalanced voltage, current, and flux vectors of the stator and rotor can be expressed as the superposition of respective positive- and negative-sequence components

$$\vec{F}^{+}_{dq} = \vec{F}^{+}_{dq+} + \vec{F}^{+}_{dq-} = \vec{F}^{+}_{dq+} + \vec{F}^{-}_{dq-}e^{-j2\omega_e t}e^{-j(\varphi_+-\varphi_-)}. \quad (3)$$

The model of DFIG in the positive- and negative-sequence synchronous reference frames has been presented in [5] and [6]. In the positive-sequence synchronous reference frame, the

relationships among the positive-sequence variables are

$$\vec{u}^{+}_{dqs+} = R_s \vec{i}^{+}_{dqs+} + \frac{d\vec{\lambda}^{+}_{dqs+}}{dt} + j\omega_e \vec{\lambda}^{+}_{dqs+} \tag{4}$$

$$\vec{u}^{+}_{dqr+} = R_r \vec{i}^{+}_{dqr+} + \frac{d\vec{\lambda}^{+}_{dqr+}}{dt} + j(\omega_e - p_n\omega_r)\vec{\lambda}^{+}_{dqr+} \tag{5}$$

$$\vec{\lambda}^{+}_{dqs+} = L_s \vec{i}^{+}_{dqs+} + L_m \vec{i}^{+}_{dqr+} \tag{6}$$

$$\vec{\lambda}^{+}_{dqr+} = L_m \vec{i}^{+}_{dqs+} + L_r \vec{i}^{+}_{dqr+}. \tag{7}$$

In the negative-sequence synchronous reference frame, the relationships among the negative-sequence variables are

$$\vec{u}^{-}_{dqs-} = R_s \vec{i}^{-}_{dqs-} + \frac{d\vec{\lambda}^{-}_{dqs-}}{dt} - j\omega_e \vec{\lambda}^{-}_{dqs-} \tag{8}$$

$$\vec{u}^{-}_{dqr-} = R_r \vec{i}^{-}_{dqr-} + \frac{d\vec{\lambda}^{-}_{dqr-}}{dt} + j(-\omega_e - p_n\omega_r)\vec{\lambda}^{-}_{dqr-} \tag{9}$$

$$\vec{\lambda}^{-}_{dqs-} = L_s \vec{i}^{-}_{dqs-} + L_m \vec{i}^{-}_{dqr-} \tag{10}$$

$$\vec{\lambda}^{-}_{dqr-} = L_m \vec{i}^{-}_{dqs-} + L_r \vec{i}^{-}_{dqr-}. \tag{11}$$

The torque and stator-side apparent power of DFIG are

$$\begin{aligned} T_e &= -1.5p_n \operatorname{Im}(\vec{\lambda}_s \hat{\vec{i}}_s) \\ &= -1.5p_n \operatorname{Im}[\vec{\lambda}^{+}_{dqs+}\hat{\vec{i}}^{+}_{dqs+} + \vec{\lambda}^{-}_{dqs-}\hat{\vec{i}}^{-}_{dqs-} \\ &\quad + \vec{\lambda}^{-}_{dqs-}\hat{\vec{i}}^{+}_{dqs+} e^{-j2\omega_e t} e^{-j(\varphi_+ - \varphi_-)} \\ &\quad + \vec{\lambda}^{+}_{dqs+}\hat{\vec{i}}^{-}_{dqs-} e^{j2\omega_e t} e^{j(\varphi_+ - \varphi_-)}] \end{aligned} \tag{12}$$

$$\begin{aligned} S_s = P_s + jQ_s &= 1.5\vec{u}_s\hat{\vec{i}}_s = 1.5[\vec{u}^{+}_{dqs+}\hat{\vec{i}}^{+}_{dqs+} + \vec{u}^{-}_{dqs-}\hat{\vec{i}}^{-}_{dqs-} \\ &\quad + \vec{u}^{-}_{dqs-}\hat{\vec{i}}^{+}_{dqs+} e^{-j2\omega_e t} e^{-j(\varphi_+ - \varphi_-)} \\ &\quad + \vec{u}^{+}_{dqs+}\hat{\vec{i}}^{-}_{dqs-} e^{j2\omega_e t} e^{j(\varphi_+ - \varphi_-)}]. \end{aligned} \tag{13}$$

III. Control-Objective Analysis Under Unbalanced Grid Voltage

The terms with complex exponents in (12) and (13) will result in torque and power pulsations at twice the grid frequency. Thus, the controller of DFIG under unbalanced grid voltage should be designed to achieve two objectives. The primary objective is to regulate the torque and stator reactive power independently, which is the exclusive objective under balanced grid voltage. The second objective is to minimize the ripples in torque and power caused by unbalanced grid voltage.

Define positive- and negative-sequence torque as

$$T_{e+} = -1.5p_n \operatorname{Im}(\vec{\lambda}^{+}_{dqs+}\hat{\vec{i}}^{+}_{dqs+}) \tag{14}$$

$$T_{e-} = -1.5p_n \operatorname{Im}(\vec{\lambda}^{-}_{dqs-}\hat{\vec{i}}^{-}_{dqs-}). \tag{15}$$

Define positive- and negative-sequence reactive power as

$$Q_{s+} = 1.5 \operatorname{Im}(\vec{u}^{+}_{dqs+}\hat{\vec{i}}^{+}_{dqs+}) \tag{16}$$

$$Q_{s-} = 1.5 \operatorname{Im}(\vec{u}^{-}_{dqs-}\hat{\vec{i}}^{-}_{dqs-}). \tag{17}$$

In the positive- and negative-sequence stator flux reference frames, respectively, both the positive- and negative-sequence components of stator flux have real parts only

$$\lambda^{+}_{ds+} = |\vec{\lambda}_{s+}| \qquad \lambda^{-}_{ds-} = |\vec{\lambda}_{s-}| \qquad \lambda^{+}_{qs+} = \lambda^{-}_{qs-} = 0. \tag{18}$$

Because of the relative high grid frequency, the voltages on stator resistances can be neglected. According to (4) and (8), the stator voltages have imaginary parts only at steady state

$$u^{+}_{qs+} = \omega_e \lambda^{+}_{ds+} \qquad u^{-}_{qs-} = -\omega_e \lambda^{-}_{ds-} \qquad u^{+}_{ds+} = u^{-}_{ds-} = 0. \tag{19}$$

Thus, (14)–(17) can be presented as

$$T_{e+} = 1.5p_n(\lambda^{+}_{ds+} i^{+}_{qs+}) \tag{20}$$

$$T_{e-} = 1.5p_n(\lambda^{-}_{ds-} i^{-}_{qs-}) \tag{21}$$

$$Q_{s+} = 1.5\omega_e(\lambda^{+}_{ds+} i^{+}_{ds+}) \tag{22}$$

$$Q_{s-} = -1.5\omega_e(\lambda^{-}_{ds-} i^{-}_{ds-}). \tag{23}$$

After stator flux oriented, the torque, stator reactive power, and active power are

$$\begin{aligned} T_e &= 1.5p_n[(\lambda^{+}_{ds+} i^{+}_{qs+} + \lambda^{-}_{ds-} i^{-}_{qs-}) \\ &\quad + (\lambda^{+}_{ds+} i^{-}_{qs-} + \lambda^{-}_{ds-} i^{+}_{qs+})\cos(2\omega_e t + \varphi_+ - \varphi_-) \\ &\quad - (\lambda^{+}_{ds+} i^{-}_{ds-} - \lambda^{-}_{ds-} i^{+}_{ds+})\sin(2\omega_e t + \varphi_+ - \varphi_-)] \end{aligned} \tag{24}$$

$$\begin{aligned} Q_s &= 1.5\omega_e[(\lambda^{+}_{ds+} i^{+}_{ds+} - \lambda^{-}_{ds-} i^{-}_{ds-}) \\ &\quad + (\lambda^{+}_{ds+} i^{-}_{ds-} - \lambda^{-}_{ds-} i^{+}_{ds+})\cos(2\omega_e t + \varphi_+ - \varphi_-) \\ &\quad + (\lambda^{+}_{ds+} i^{-}_{qs-} + \lambda^{-}_{ds-} i^{+}_{qs+})\sin(2\omega_e t + \varphi_+ - \varphi_-)] \end{aligned} \tag{25}$$

$$\begin{aligned} P_s &= 1.5\omega_e[(\lambda^{+}_{ds+} i^{+}_{qs+} - \lambda^{-}_{ds-} i^{-}_{qs-}) \\ &\quad + (\lambda^{+}_{ds+} i^{-}_{qs-} - \lambda^{-}_{ds-} i^{+}_{qs+})\cos(2\omega_e t + \varphi_+ - \varphi_-) \\ &\quad + (-\lambda^{+}_{ds+} i^{-}_{ds-} - \lambda^{-}_{ds-} i^{+}_{ds+})\sin(2\omega_e t + \varphi_+ - \varphi_-)]. \end{aligned} \tag{26}$$

According to (24) and (25), in order to minimize the ripples in torque and stator reactive power, following equations should be satisfied:

$$\lambda^{+}_{ds+} i^{-}_{qs-} = -\lambda^{-}_{ds-} i^{+}_{qs+} \tag{27}$$

$$\lambda^{+}_{ds+} i^{-}_{ds-} = \lambda^{-}_{ds-} i^{+}_{ds+}. \tag{28}$$

Multiplying both sides of (27) and (28) with $\lambda^{+}_{ds+}\lambda^{-}_{ds-}$, and rearranging, we get

$$\lambda^{-}_{ds-} i^{-}_{qs-} = -\left(\frac{\lambda^{-}_{ds-}}{\lambda^{+}_{ds+}}\right)^2 \lambda^{+}_{ds+} i^{+}_{qs+} \tag{29}$$

$$\lambda^{-}_{ds-} i^{-}_{ds-} = \left(\frac{\lambda^{-}_{ds-}}{\lambda^{+}_{ds+}}\right)^2 \lambda^{+}_{ds+} i^{+}_{ds+}. \tag{30}$$

Substituting (20)–(23) into (29) and (30), we get

$$T_{e-} = -\left(\frac{\lambda^-_{ds-}}{\lambda^+_{ds+}}\right)^2 T_{e+} \tag{31}$$

$$Q_{s-} = -\left(\frac{\lambda^-_{ds-}}{\lambda^+_{ds+}}\right)^2 Q_{s+}. \tag{32}$$

According to (26), in order to minimize the ripples in stator active power, following equations should be satisfied:

$$\lambda^+_{ds+} i^-_{qs-} = \lambda^-_{ds-} i^+_{qs+} \tag{33}$$

$$\lambda^+_{ds+} i^-_{ds-} = -\lambda^-_{ds-} i^+_{ds+}. \tag{34}$$

Using the same deductive process as earlier, we get

$$T_{e-} = \left(\frac{\lambda^-_{ds-}}{\lambda^+_{ds+}}\right)^2 T_{e+} \tag{35}$$

$$Q_{s-} = \left(\frac{\lambda^-_{ds-}}{\lambda^+_{ds+}}\right)^2 Q_{s+}. \tag{36}$$

According to earlier analysis, two controllers are required. The positive-sequence controller implements the decoupled control of torque and reactive power as the controller does under balanced grid voltage. The negative-sequence controller regulates the negative-sequence torque and reactive power to follow the reference values, which are given by (31) and (32) with the objective to minimize the ripples in torque and stator reactive power, or by (35) and (36) with the objective to minimize the ripples in stator active power.

IV. Positive-Sequence Controller Design

A. Controlled Plant Analysis

In order to choose appropriate input–output control pairs in DFIG under unbalanced grid voltage, the relative gain array (RGA) methodology [16] is used to calculate the degrees of relevance between the input and output variables.

The RGA is calculated as the element-by-element product of the system transfer matrix and the inverse of its transposed matrix. A large RGA element indicates that corresponding input and output variables are relevant, while a small RGA element shows a low correlation between corresponding input and output variables [17].

Substituting (6) and (7) into (5), and rearranging, we get

$$\vec{u}^+_{dqr+} = \left(\frac{R_r}{L_m}\right)\vec{\lambda}^+_{dqs+} - \left(\frac{R_r L_s}{L_m}\right)\vec{i}^+_{dqs+} + L_{\sigma m}\frac{d\vec{i}^+_{dqs+}}{dt} + j\omega_{\text{slip}+} L_{\sigma m}\vec{i}^+_{dqs+} + j\omega_{\text{slip}+}\left(\frac{L_r}{L_m}\right)\vec{\lambda}^+_{dqs+} \tag{37}$$

where $L_{\sigma m} = (L_m - L_r L_s / L_m)$, and $\omega_{\text{slip}+} = (\omega_e - p_n \omega_r)$.

Substituting (20) and (22) into (37), and then separating the result into real and imaginary parts, the Laplace equations relating the positive-sequence variables are

$$\frac{1}{1.5 p_n \omega_e \lambda^+_{ds+}} \begin{bmatrix} \left(L_{\sigma m} s - \dfrac{R_r L_s}{L_m}\right)\omega_e & p_n \omega_{\text{slip}+} L_{\sigma m} \\ -\omega_e \omega_{\text{slip}+} L_{\sigma m} & \left(L_{\sigma m} s - \dfrac{R_r L_s}{L_m}\right) p_n \end{bmatrix} \cdot \begin{bmatrix} T_{e+} \\ Q_{s+} \end{bmatrix} = \begin{bmatrix} u^+_{qr+} \\ u^+_{dr+} \end{bmatrix} - \begin{bmatrix} \omega_{\text{slip}+}\left(\dfrac{L_r}{L_m}\right)\lambda^+_{ds+} \\ \left(\dfrac{R_r}{L_m}\right)\lambda^+_{ds+} \end{bmatrix}. \tag{38}$$

The perturbed form of (38) is

$$\frac{1}{1.5 p_n \omega_e \lambda^+_{ds+}} \begin{bmatrix} \left(L_{\sigma m} s - \dfrac{R_r L_s}{L_m}\right)\omega_e & p_n \omega_{\text{slip}+} L_{\sigma m} \\ -\omega_e \omega_{\text{slip}+} L_{\sigma m} & \left(L_{\sigma m} s - \dfrac{R_r L_s}{L_m}\right) p_n \end{bmatrix} \cdot \begin{bmatrix} \delta T_{e+} \\ \delta Q_{s+} \end{bmatrix} = \begin{bmatrix} \delta u^+_{qr+} \\ \delta u^+_{dr+} \end{bmatrix}. \tag{39}$$

The RGA of the matrix in (39) is

$$\begin{bmatrix} \left(L_{\sigma m} s - \dfrac{R_r L_s}{L_m}\right)\omega_e & p_n \omega_{\text{slip}+} L_{\sigma m} \\ -\omega_e \omega_{\text{slip}+} L_{\sigma m} & \left(L_{\sigma m} s - \dfrac{R_r L_s}{L_m}\right) p_n \end{bmatrix} \cdot \times \left(\begin{bmatrix} \left(L_{\sigma m} s - \dfrac{R_r L_s}{L_m}\right)\omega_e & p_n \omega_{\text{slip}+} L_{\sigma m} \\ -\omega_e \omega_{\text{slip}+} L_{\sigma m} & \left(L_{\sigma m} s - \dfrac{R_r L_s}{L_m}\right) p_n \end{bmatrix}^T \right)^{-1}$$

$$= \frac{1}{(L_{\sigma m} s - R_r L_s / L_m)^2 + (\omega_{\text{slip}+} L_{\sigma m})^2} \times \begin{bmatrix} \left(L_{\sigma m} s - \dfrac{R_r L_s}{L_m}\right)^2 & (\omega_{\text{slip}+} L_{\sigma m})^2 \\ (\omega_{\text{slip}+} L_{\sigma m})^2 & \left(L_{\sigma m} s - \dfrac{R_r L_s}{L_m}\right)^2 \end{bmatrix} \tag{40}$$

where ".×" means element-by-element multiplication.

Since the RGA is only used to analyze the DFIG model, it is sufficient to be evaluated at zero frequency to give valid input–output pairs at steady state [16].

If the slip speed of DFIG is in ±0.2 of the synchronous speed, substituting the parameters from the appendix, the diagonal RGA elements are between 0.8711 and 1, while the values of the off-diagonal elements are between 0.1289 and 0. The diagonal elements are much larger than the off-diagonal elements. Hence, the positive-sequence torque should be controlled by the rotor *q*-axis voltage, and the positive-sequence reactive power should be controlled by the rotor *d*-axis voltage. The conclusion is consistent with the situation under balanced grid voltage [2].

Rearranging (38), the differential equations representing the dynamic response of direct torque/reactive power control are

$$\frac{dT_{e+}}{dt} = 1.5p_n\lambda^+_{ds+}\left(\frac{u^+_{qr+}}{L_{\sigma m}} + \frac{R_rL_s}{L_{\sigma m}L_m}\frac{T_{e+}}{1.5p_n\lambda^+_{ds+}} - \frac{\omega_{\text{slip}+}L_r\lambda^+_{ds+}}{L_{\sigma m}L_m} - \frac{\omega_{\text{slip}+}Q_{s+}}{1.5\omega_e\lambda^+_{ds+}}\right) \quad (41)$$

$$\frac{dQ_{s+}}{dt} = 1.5\omega_e\lambda^+_{ds+}\left(\frac{u^+_{dr+}}{L_{\sigma m}} + \frac{R_rL_s}{L_{\sigma m}L_m}\frac{Q_{s+}}{1.5\omega_e\lambda^+_{ds+}} - \frac{R_r\lambda^+_{ds+}}{L_{\sigma m}L_m} + \frac{\omega_{\text{slip}+}T_{e+}}{1.5p_n\lambda^+_{ds+}}\right). \quad (42)$$

B. Parametric Uncertainty

The parameters of the DFIG are obtained by identification experiments in which errors are unavoidable, and furthermore, these parameters may vary with ambient temperature and magnetic saturation. Considering the uncertainties of the machine parameters, it is assumed that the parameters in (41) and (42) are bounded as follows:

$$R_{r\min} < R_r = R_{r0} + \Delta R_r < R_{r\max}$$
$$L_{m\min} < L_m = L_{m0} + \Delta L_m < L_{m\max}$$
$$L_{s\min} < L_s = L_{s0} + \Delta L_s < L_{s\max}$$
$$L_{r\min} < L_r = L_{r0} + \Delta L_r < L_{r\max}$$

where R_{r0}, L_{m0}, L_{s0}, and L_{r0} denote nominal values, and R_r, L_m, L_s, and L_r denote actual values.

C. Integral Sliding-Mode Controller Design

Sliding-mode controller enforces the system state on the predefined sliding surface in the system state space by adaptively changing the structure of the controller. Hence, the system response depends only on the sliding surface and is insensitive to variations of system parameters and external disturbances [8].

The sliding surfaces are chosen as

$$s_{Te+} = x_{Te+} + c\int_{-\infty}^{t} x_{Te+}(z)dz_{Te+} = 0 \quad (43)$$

$$s_{Qs+} = x_{Qs+} + c\int_{-\infty}^{t} x_{Qs+}(z)dz_{Qs+} = 0 \quad (44)$$

where c is the coefficient of the sliding surface, z_{Te+}, z_{Qs+} are the dummy variables for the integration, and state variables x_{Te+}, x_{Qs+} are the errors between reference values and real values

$$x_{Te+} = T^*_{e+} - T_{e+} \quad (45)$$

$$x_{Qs+} = Q^*_{s+} - Q_{s+}. \quad (46)$$

In order to guarantee complete robustness during the entire response, the system states can be set in the sliding surfaces without the reaching phase, which will be achieved by choosing the initial conditions of the integrators as

$$\int_{-\infty}^{0} x_{Te+}(z)dz_{Te+} = -\frac{x_{Te0+}}{c} \quad (47)$$

$$\int_{-\infty}^{0} x_{Qs+}(z)dz_{Qs+} = -\frac{x_{Qs0+}}{c} \quad (48)$$

where x_{Te0+} and x_{Qs0+} are the initial conditions of x_{Te+} and x_{Qs+}.

The outputs of the sliding-mode controllers consist of equivalent controls and switching controls

$$u^+_{qr+} = u^{\text{eq}+}_{qr+} - \Delta u^+_{qr+} \quad (49)$$

$$u^+_{dr+} = u^{\text{eq}+}_{dr+} - \Delta u^+_{dr+}. \quad (50)$$

The equivalent controls are used to control the nominal plant model, and the switching controls are added to ensure the desired performance despite parametric uncertainty.

By using the condition of the equivalent controls as $\dot{s} = 0$, the equivalent controls are derived as

$$u^{\text{eq}+}_{qr+} = \frac{L_{\sigma m0}}{1.5p_n\lambda^+_{ds+}}\frac{dT^*_{e+}}{dt} + \frac{L_{\sigma m0}cx_{Te+}}{1.5p_n\lambda^+_{ds+}} - \frac{R_{r0}L_{s0}}{L_{m0}}\frac{T_{e+}}{1.5p_n\lambda^+_{ds+}} + \frac{L_{r0}}{L_{m0}}\omega_{\text{slip}+}\lambda^+_{ds+} + L_{\sigma m0}\frac{\omega_{\text{slip}+}Q_{s+}}{1.5\omega_e\lambda^+_{ds+}} \quad (51)$$

$$u^{\text{eq}+}_{dr+} = \frac{L_{\sigma m0}}{1.5\omega_e\lambda^+_{ds+}}\frac{dQ^*_{s+}}{dt} + \frac{L_{\sigma m0}cx_{Qs+}}{1.5\omega_e\lambda^+_{ds+}} - \frac{R_{r0}L_{s0}}{L_{m0}}\frac{Q_{s+}}{1.5\omega_e\lambda^+_{ds+}} + \frac{R_{r0}}{L_{m0}}\lambda^+_{ds+} - L_{\sigma m0}\frac{\omega_{\text{slip}+}T_{e+}}{1.5p_n\lambda^+_{ds+}}. \quad (52)$$

The switching controls are

$$\Delta u^+_{qr+} = K_{Te1+}x_{Te+}\text{sign}(s_{Te+}x_{Te+}) + K_{Te2+}\text{sign}(s_{Te+}) \quad (53)$$

$$\Delta u^+_{dr+} = K_{Qs1+}x_{Qs+}\text{sign}(s_{Qs+}x_{Qs+}) + K_{Qs2+}\text{sign}(s_{Qs+}). \quad (54)$$

The constants K in (53) and (54) are determined by the Lyapunov stability condition as

$$s_{Te+}\dot{s}_{Te+} < 0 \quad (55)$$

$$s_{Qs+}\dot{s}_{Qs+} < 0. \quad (56)$$

The constants to satisfy the inequality given in (55) are

$$K_{Te1+} > \max\left|\frac{c}{1.5p_n\lambda^+_{ds+}}(L_{\sigma m0} - L_{\sigma m})\right| \quad (57)$$

$$K_{Te2+} > \max\left|\frac{(L_{\sigma m0} - L_{\sigma m})}{1.5p_n\lambda^+_{ds+}}\frac{dT^*_{e+}}{dt} + \left(\frac{R_rL_s}{L_m} - \frac{R_{r0}L_{s0}}{L_{m0}}\right)\frac{T_{e+}}{1.5p_n\lambda^+_{ds+}}\right.$$

$$+ (L_{\sigma m0} - L_{\sigma m}) \frac{\omega_{\text{slip}+}}{1.5\lambda^+_{ds+}\omega_e} Q_{s+} + \left(\frac{L_{r0}}{L_{m0}} - \frac{L_r}{L_m} \right) \omega_{\text{slip}+} \lambda^+_{ds+} \Bigg|. \quad (58)$$

The constants to satisfy the inequality given in (56) are

$$K_{Qs1+} > \max \left| \frac{c}{1.5\omega_e \lambda^+_{ds+}} (L_{\sigma m0} - L_{\sigma m}) \right| \quad (59)$$

$$K_{Qs2+} > \max \Bigg| \frac{(L_{\sigma m0} - L_{\sigma m})}{1.5\omega_e \lambda^+_{ds+}} \frac{dQ^*_{s+}}{dt} + \left(\frac{R_r L_s}{L_m} - \frac{R_{r0} L_{s0}}{L_{m0}} \right) \frac{Q_{s+}}{1.5\omega_e \lambda^+_{ds+}} + (L_{\sigma m} - L_{\sigma m0}) \frac{\omega_{\text{slip}+}}{1.5 p_n \lambda^+_{ds+}} T_{e+} + \left(\frac{R_{r0}}{L_{m0}} - \frac{R_r}{L_m} \right) \lambda^+_{ds+} \Bigg|. \quad (60)$$

In (58) and (60), dT^*_{e+}/dt and dQ^*_{s+}/dt will be infinite if the reference values are abruptly changed, and hence, K_{Te2+} and K_{Qs2+} cannot be determined if parametric uncertainty is considered. Therefore, the rising and falling rates of input reference signals should be limited. Practically, in practical engineering implementations, rate limiters are also need to avoid large stress on mechanical and/or electrical components.

The switching actions in (53) and (54) will result in chattering phenomenon. It can be conquered by boundary layer solution, which replaces the sign functions with saturation functions in a small vicinity of the sliding surface. Hence, control discontinuities and switching actions in the control loop are avoided.

Parametric uncertainties defined in Section IV-B are included in the design process of sliding-mode control scheme as explained here. The nominal parameters are used to generate equivalent controls given as (51) and (52) to control the nominal plant model. The bounds of parametric uncertainties are used to determine the coefficients of switching controls to guarantee that Lyapunov stability conditions given in (55) and (56) are fulfilled, when parametric errors exist. The coefficients of switching controls are determined according to (57)–(60).

V. Negative-Sequence Controller Design

Substituting (10) and (11) into (9), and rearranging gives

$$\vec{u}^-_{dqr-} = \left(\frac{R_r}{L_m} \right) \vec{\lambda}^-_{dqs-} - \left(\frac{R_r L_s}{L_m} \right) \vec{i}^-_{dqs-} + L_{\sigma m} \frac{d\vec{i}^-_{dqs-}}{dt} + j\omega_{\text{slip}-} L_{\sigma m} \vec{i}^-_{dqs-} + j\omega_{\text{slip}-} \left(\frac{L_r}{L_m} \right) \vec{\lambda}^-_{dqs-} \quad (61)$$

where $\omega_{\text{slip}-} = (-\omega_e - p_n \omega_r)$.

Substituting (21) and (23) into (61), and then separating the result into real and imaginary parts, the Laplace equations relating the negative-sequence variables are

$$\frac{1}{1.5 p_n \omega_e \lambda^-_{ds-}} \times \begin{bmatrix} \left(L_{\sigma m} s - \frac{R_r L_s}{L_m} \right) \omega_e & -p_n \omega_{\text{slip}-} L_{\sigma m} \\ -\omega_e \omega_{\text{slip}-} L_{\sigma m} & -\left(L_{\sigma m} s - \frac{R_r L_s}{L_m} \right) p_n \end{bmatrix} \cdot \begin{bmatrix} T_{e-} \\ Q_{s-} \end{bmatrix} = \begin{bmatrix} u^-_{qr-} \\ u^-_{dr-} \end{bmatrix} - \begin{bmatrix} \omega_{\text{slip}-} \left(\frac{L_r}{L_m} \right) \lambda^-_{ds-} \\ \left(\frac{R_r}{L_m} \right) \lambda^-_{ds-} \end{bmatrix}. \quad (62)$$

The perturbed form of (62) is

$$\frac{1}{1.5 p_n \omega_e \lambda^-_{ds-}} \times \begin{bmatrix} \left(L_{\sigma m} s - \frac{R_r L_s}{L_m} \right) \omega_e & -p_n \omega_{\text{slip}-} L_{\sigma m} \\ -\omega_e \omega_{\text{slip}-} L_{\sigma m} & -\left(L_{\sigma m} s - \frac{R_r L_s}{L_m} \right) p_n \end{bmatrix} \cdot \begin{bmatrix} \delta T_{e-} \\ \delta Q_{s-} \end{bmatrix} = \begin{bmatrix} \delta u^-_{qr-} \\ \delta u^-_{dr-} \end{bmatrix}. \quad (63)$$

The RGA of the matrix in (63) is

$$\begin{bmatrix} \left(L_{\sigma m} s - \frac{R_r L_s}{L_m} \right) \omega_e & -p_n \omega_{\text{slip}-} L_{\sigma m} \\ -\omega_e \omega_{\text{slip}-} L_{\sigma m} & -\left(L_{\sigma m} s - \frac{R_r L_s}{L_m} \right) p_n \end{bmatrix} \cdot \times \left(\begin{bmatrix} \left(L_{\sigma m} s - \frac{R_r L_s}{L_m} \right) \omega_e & -p_n \omega_{\text{slip}-} L_{\sigma m} \\ -\omega_e \omega_{\text{slip}-} L_{\sigma m} & -\left(L_{\sigma m} s - \frac{R_r L_s}{L_m} \right) p_n \end{bmatrix}^T \right)^{-1} = \frac{1}{(L_{\sigma m} s - R_r L_s / L_m)^2 + (\omega_{\text{slip}-} L_{\sigma m})^2} \times \begin{bmatrix} \left(L_{\sigma m} s - \frac{R_r L_s}{L_m} \right)^2 & (\omega_{\text{slip}-} L_{\sigma m})^2 \\ (\omega_{\text{slip}-} L_{\sigma m})^2 & \left(L_{\sigma m} s - \frac{R_r L_s}{L_m} \right)^2 \end{bmatrix}. \quad (64)$$

If the slip speed of DFIG is in ± 0.2 of synchronous speed, substituting the parameters from the appendix, the diagonal RGA elements are between 0.0529 and 0.0770, while the values of the off-diagonal elements are between 0.9471 and 0.9230. The off-diagonal elements are much larger than the diagonal elements. Hence, the negative-sequence torque should be controlled by the rotor d-axis voltage, and the negative-sequence reactive power should be controlled by the rotor q-axis voltage, which is different from the positive-sequence case.

Because there are no transient terms in the off-diagonal elements of (63), only integral controllers shown in (65) and (66) are adequate to achieve first order dynamic responses in

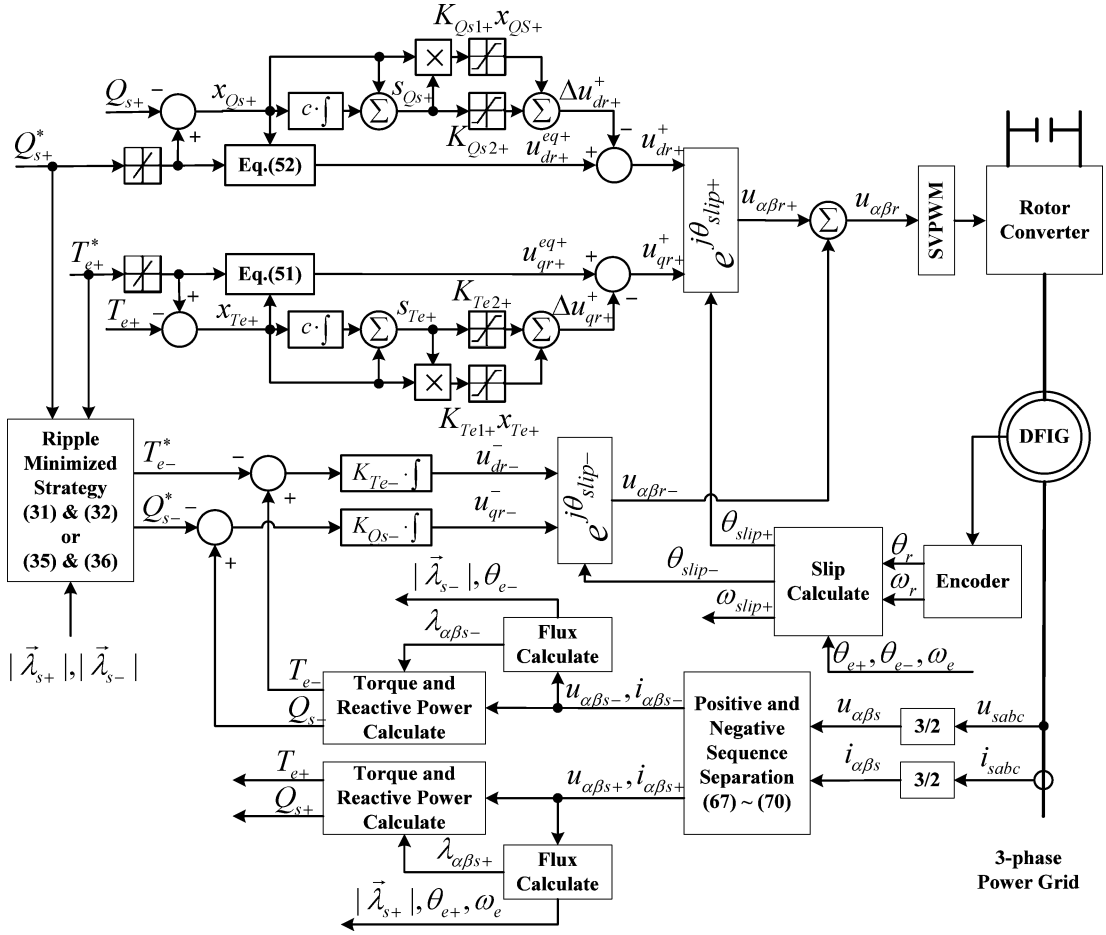

Fig. 2. Proposed ISM-DTC scheme of DFIG under unbalanced grid voltage.

closed-loop system

$$u_{dr-}^{-} = K_{Te-}\int (T_{e-} - T_{e-}^{*})dt \tag{65}$$

$$u_{qr-}^{-} = K_{Qs-}\int (Q_{s-} - Q_{s-}^{*})dt. \tag{66}$$

VI. System Implementation

The proposed control scheme requires fast and accurate decomposition of positive- and negative-sequence components. There are usually two methods [7]. The first one is using filters to bypass dc components and suppress double-frequency components in positive- and negative-sequence synchronous rotating reference frames. The second one is based on signal delay cancellation. The positive- and negative-sequence components are calculated by adding or subtracting the present real-time signal with the signal delayed for a quarter of period in the stationary α–β reference frame. The second method is adopted in this research, and the decomposition algorithm is given as

$$F_{\alpha+}(t) = \frac{1}{2}[F_{\alpha}(t) - F_{\beta}(t - \pi/2\omega_e)] \tag{67}$$

$$F_{\beta+}(t) = \frac{1}{2}[F_{\beta}(t) + F_{\alpha}(t - \pi/2\omega_e)] \tag{68}$$

$$F_{\alpha-}(t) = \frac{1}{2}[F_{\alpha}(t) + F_{\beta}(t - \pi/2\omega_e)] \tag{69}$$

$$F_{\beta-}(t) = \frac{1}{2}[F_{\beta}(t) - F_{\alpha}(t - \pi/2\omega_e)]. \tag{70}$$

Fig. 2 shows the block diagram of the proposed ISM-DTC scheme of DFIG under unbalanced grid voltage. The positive- and negative-sequence components of stator flux, torque, and reactive power are calculated in the stationary α–β reference frame using respective positive- and negative-sequence components of stator voltage and current as follows

$$\lambda_{\alpha\beta s\pm} = \int (u_{\alpha\beta s\pm} - R_s i_{\alpha\beta s\pm})dt \tag{71}$$

$$T_{e\pm} = 1.5p_n(\lambda_{\alpha s\pm} i_{\beta s\pm} - \lambda_{\beta s\pm} i_{\alpha s\pm}) \tag{72}$$

$$Q_{s\pm} = 1.5(u_{\beta s\pm} i_{\alpha s\pm} - u_{\alpha s\pm} i_{\beta s\pm}). \tag{73}$$

As mentioned in (18), in the stator flux reference frame, the *d*-axes flux equals to flux magnitudes and the *q*-axes flux is zero, hence the flux magnitudes and angles have to be evaluated with (71). The control algorithms shown in (43)–(54), (65), and (66) do not include stator *d*–*q* axis voltage and current, and the torque and reactive power feedback is calculated in the stationary α–β

reference frame, hence the coordinate transformations and *d–q* decomposition of stator voltage and current are eliminated.

Since the torque and reactive power are directly controlled by rotor voltage, the rotor current is not present in the control arithmetic, which eliminates the measurement, coordinate transformation and sequence decomposition of rotor current. Hence, the control algorithm is simpler than the cascaded PI control scheme proposed in [5], in which the rotor current should be measured, coordinate transformed and decomposed into positive- and negative-sequence components.

VII. Simulation Results

The proposed ISM-DTC scheme is simulated with MATLAB/Simulink. The nominal parameters of DFIG are shown in the Appendix. The rising and falling rate of positive-sequence torque and reactive power reference input is limited at ±25 N·m/s and ±5000 var/s, respectively. The value of sliding surface coefficient c is chosen as 20. To determine the switching control, the bounds of parametric uncertainties are assumed as $0.5R_{r0} \le R_r \le 1.5R_{r0}$, $0.5L_{m0} \le L_m \le 1.5L_{m0}$, $0.5L_{r0} \le L_r \le 1.5L_{r0}$, and $0.5L_{s0} \le L_s \le 1.5L_{s0}$. Under these assumptions and according to (57)–(60), the constants in (53) and (54) can be chosen as $K_{Te1+} = 0.152$, $K_{Te2+} = 45.15$, $K_{Qs1+} = 0.001$, and $K_{Qs2+} = 75.95$. The constants of the integral controllers in (65) and (66) are chosen as $K_{Te-} = 1624$, $K_{Qs-} = 10.34$.

In all the simulations, the voltages of phases A and B are kept at the rated values and the voltage of phase C is reduced to provide a three-phase unbalanced supply voltage. The ratio of negative-sequence to positive-sequence voltage is 10%. The torque reference value is step-changed from 0 to –5 N·m at 0.1 s, while the reactive power reference is kept at 1000 var.

Fig. 3 shows the simulation results with the torque and reactive power ripple-minimized strategy. The torque of DFIG tracks the reference value and the stator reactive power remains almost unchanged. The average value of the stator active power changes with the torque. The ripples in torque and reactive power are effectively minimized, but the active power pulsations are at twice the grid frequency. Because the magnitude of the generator torque increases, the generator decelerates from super-synchronous speed to subsynchronous speed, which does not influence the control performance. Fig. 4 shows the simulation results with the active power ripple-minimized strategy. In contrast with Fig. 3, the ripples in active power are effectively minimized, but the torque and reactive power pulsations are at twice the grid frequency.

To show the parametric robustness of the proposed ISM-DTC scheme, the magnetizing inductance of the DFIG is set to 50% and 150% of nominal value, respectively. The simulation results are shown in Fig. 5 with torque and reactive power ripple-minimized strategy, and in Fig. 6 with active power ripple-minimized strategy. Even with so large inductance error, the ripples in torque and power are still effectively minimized by corresponding control strategies, and there is hardly any difference in the responses. The rotor winding resistance of the DFIG is also set to 50% and 150% of nominal value, respectively.

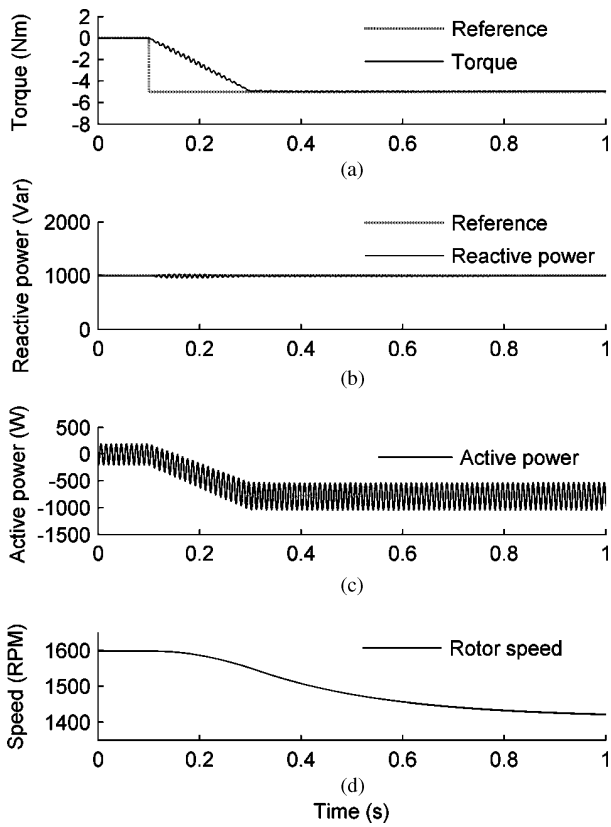

Fig. 3. Simulation results with torque and reactive power ripple-minimized strategy.

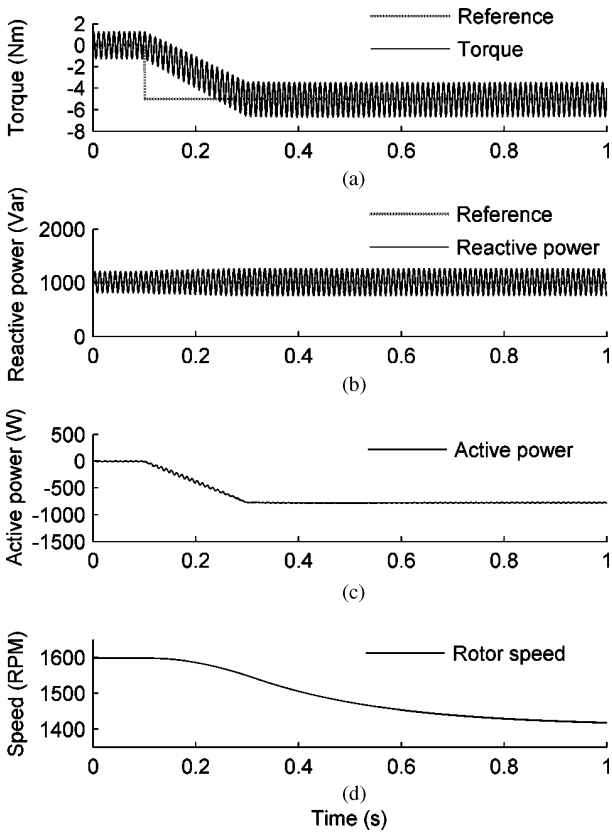

Fig. 4. Simulation results with active power ripple-minimized strategy.

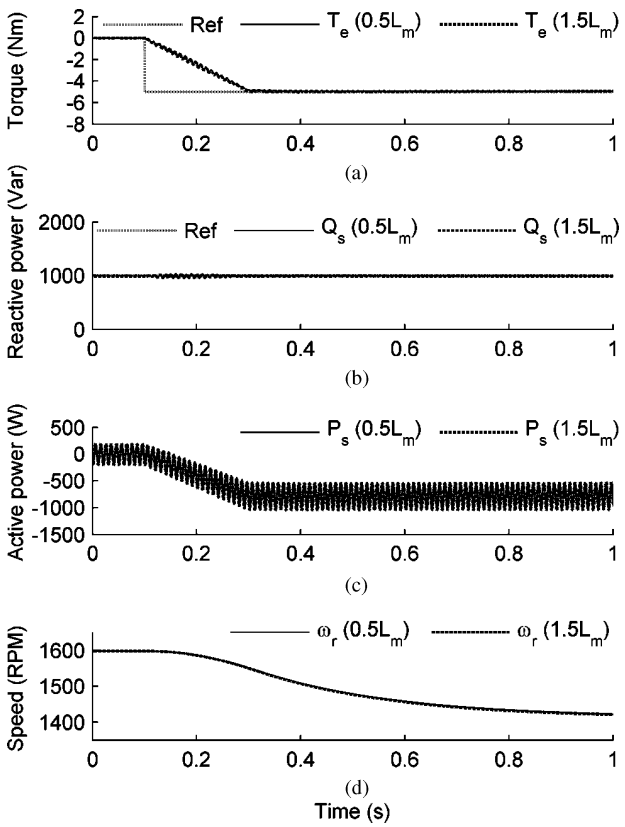

Fig. 5. Simulation results with torque and reactive power ripple-minimized strategy under magnetizing inductance errors.

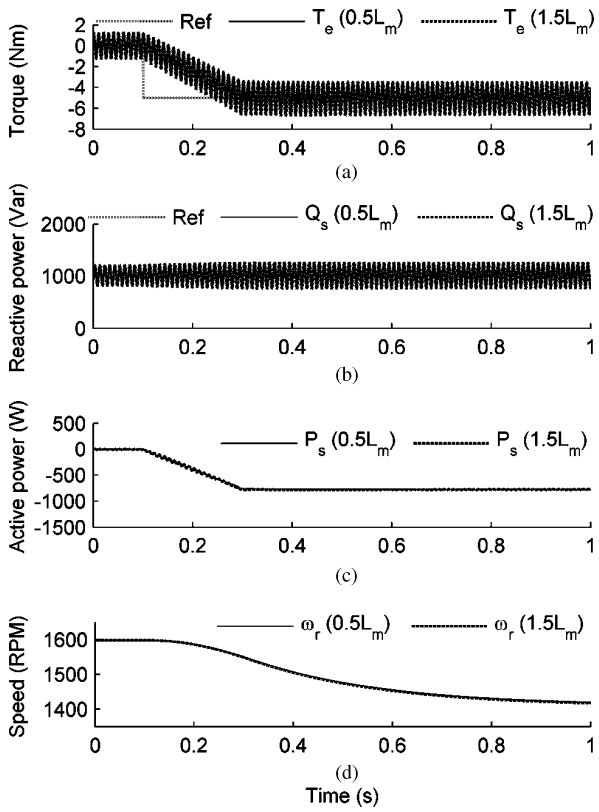

Fig. 6. Simulation results with active power ripple-minimized strategy under magnetizing inductance errors.

The responses of both control strategies shown in Figs. 7 and 8 verify the parametric robustness of the proposed scheme again.

VIII. Hardware Experimental Results

Fig. 9 shows the configuration of the hardware experimental system. The rotor shaft of the DFIG is mechanically coupled with a separately excited dc motor, whose armature and field voltages can be manually adjusted to emulate a variable-speed prime mover with linear torque–speed characteristics. The A-phase and B-phase stator windings of the DFIG are directly connected to the three-phase grid, and the C-phase stator winding is connected to the grid through an autotransformer. The autotransformer is manually adjusted to reduce the voltage to provide a three-phase unbalanced supply voltage. The ratio of negative-sequence to positive-sequence voltage is 10%. The rotor converter is an integrated power module (IPM) based inverter controlling the voltage applied to the rotor winding of the DFIG. The dSpace DS1103 is a prototyping card installed in a PC. It acquires stator voltages, stator currents, and rotor position from the sensors and the encoder at a rate of 5 kHz, and processes them with the proposed control algorithm. The card then generates 10 kHz space vector pulsewidth modulation (SVPWM) switching signal for the rotor convertor control. The operating conditions and signals are displayed and stored in the PC in which the prototyping card is installed. The parameters of the DFIG are shown in the Appendix.

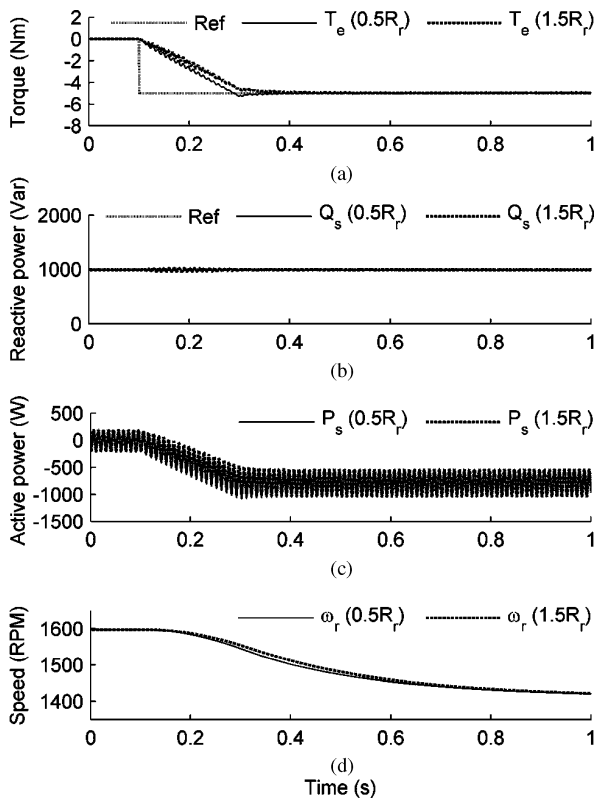

Fig. 7. Simulation results with torque and reactive power ripple-minimized strategy under rotor resistance errors.

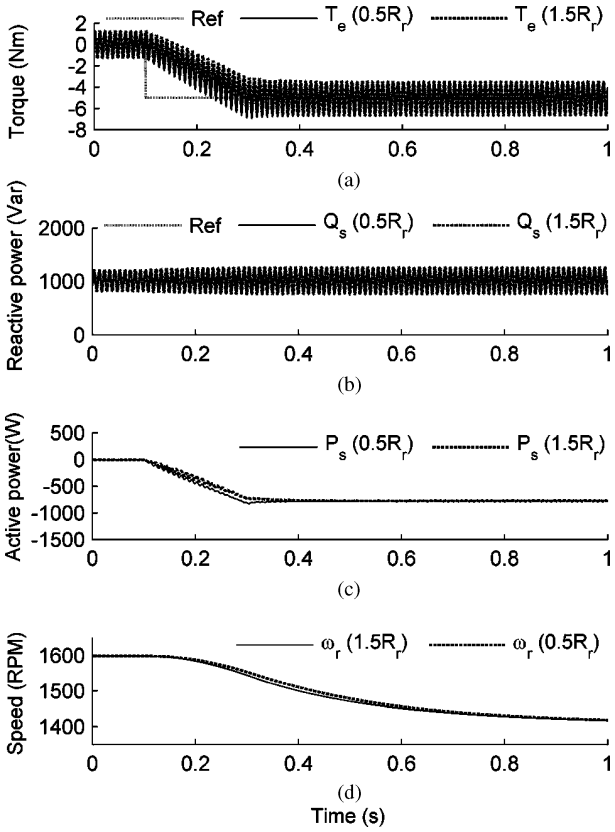

Fig. 8. Simulation results with active power ripple-minimized strategy under rotor resistance errors.

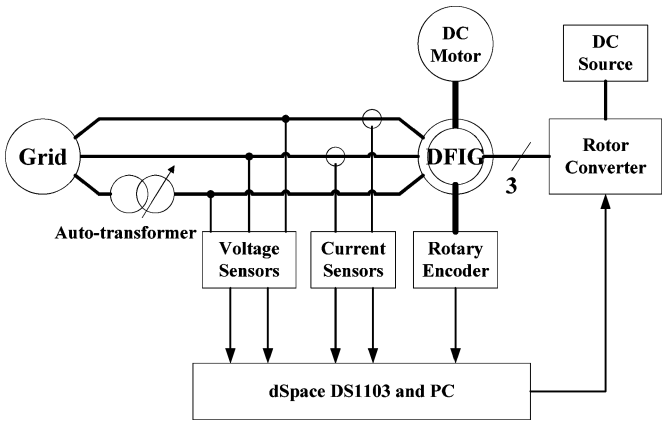

Fig. 9. Configuration of experimental system.

Fig. 10 shows the experimental results with the torque and reactive power ripple-minimized strategy. The torque reference value is step-changed from 0 to –5 N·m at 0.1 s, while the reactive power reference is kept at 1000 var. The torque of DFIG tracks the reference value and the stator reactive power remains almost unchanged. The ripples in torque and reactive power are effectively minimized, but the active power pulsations are at twice the grid frequency. Fig. 11 shows the experimental results with the active power ripple-minimized strategy. In contrast with Fig. 10, the ripples in active power are effectively minimized, but the torque and reactive power pulsations are at twice the grid frequency. The experimental results are very similar to

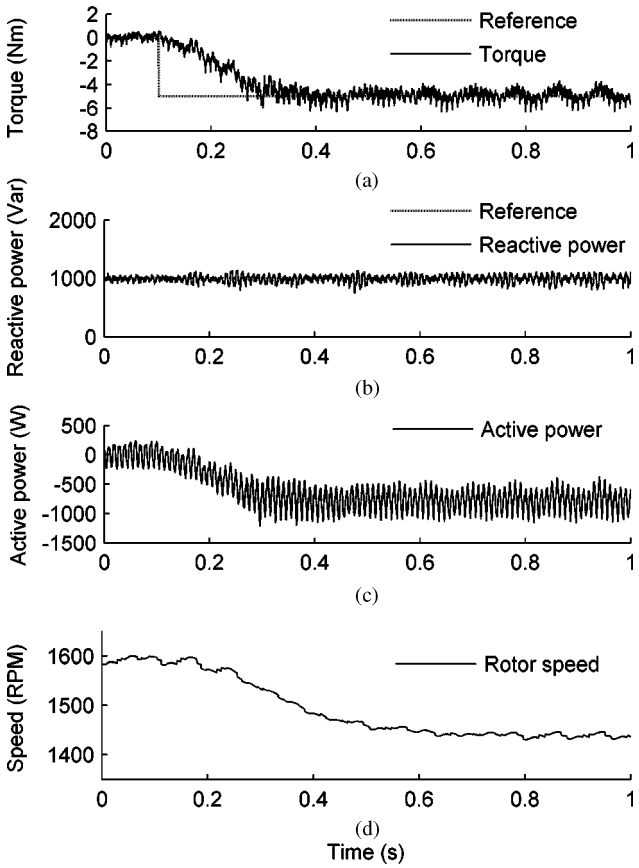

Fig. 10. Experimental results with torque and reactive power ripple-minimized strategy.

corresponding simulation results, which prove that the practical characteristics are identical with theoretical derivations.

To compare the proposed ISM-DTC scheme with traditional control schemes, experiments of two cascaded PI control schemes are also carried out on the same hardware system.

First, the experiment of the cascaded PI control scheme without positive- and negative-sequence separation, as proposed in [2], is carried out. The PI controllers of inner current loop and outer torque/reactive power loop are both designed to obtain first-order closed-loop responses, whose time constants are 10 and 50 ms, respectively. Fig. 12 shows the harmonic spectrum of torque, reactive power, and active power of the DFIG operating with a torque of –8 N·m and a reactive power of 1000 var. With traditional control scheme proposed in [2], the magnitudes of the 100 Hz ripples in torque, reactive power, and active power are 93%, 76%, and 76% of their respective average values. With torque and reactive power ripple-minimized strategy, the corresponding ratio is reduced to 3%, 3%, and 18%, respectively. With active power ripple-minimized strategy, the corresponding ratio is reduced to 21%, 21%, and 2%, respectively.

To understand why the torque and power ripples are so drastically reduced with the same PWM and switching frequency, we can refer to (20)–(36). If the relationship between the positive-sequence and negative-sequence torque satisfies (31) and the relationship between positive-sequence and negative-sequence

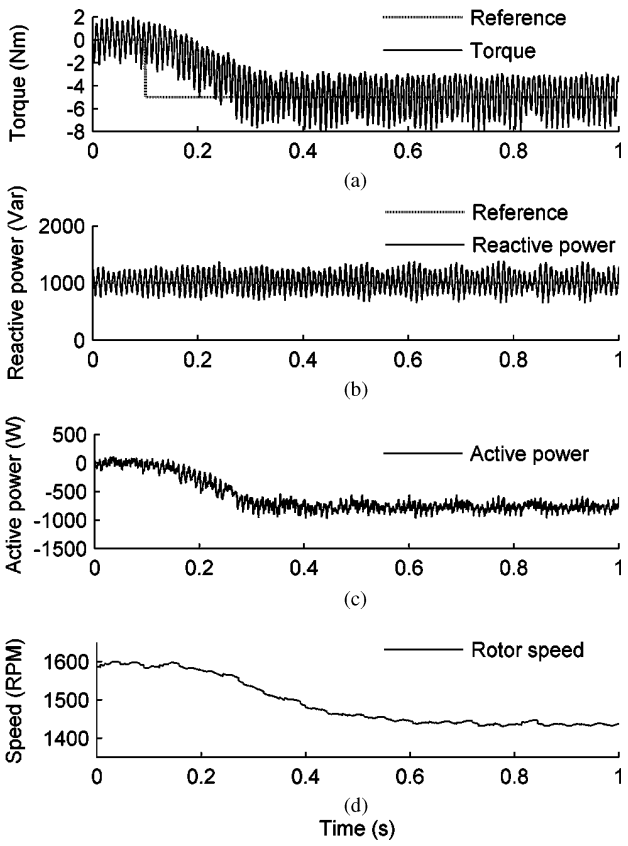

Fig. 11. Experimental results with active power ripple-minimized strategy.

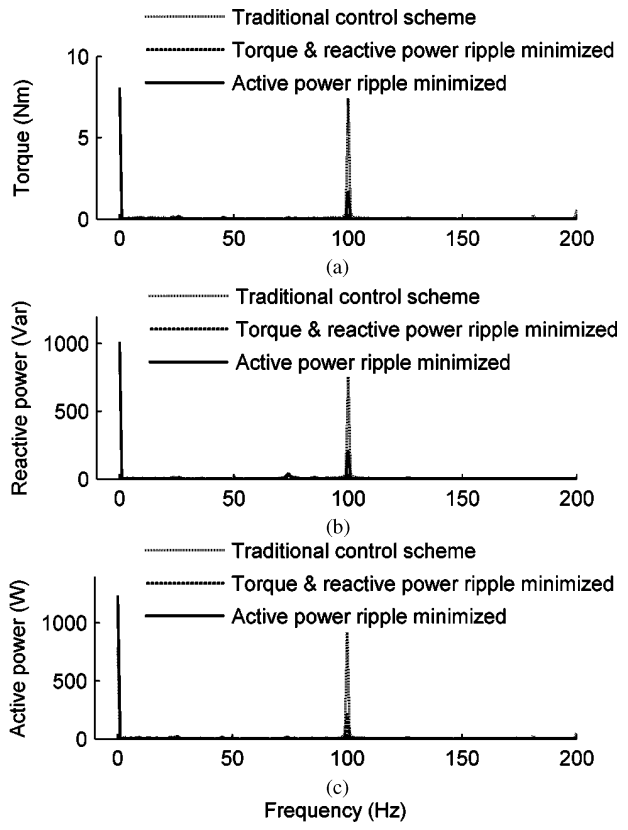

Fig. 12. Harmonic spectrum comparison of torque, reactive, and active power.

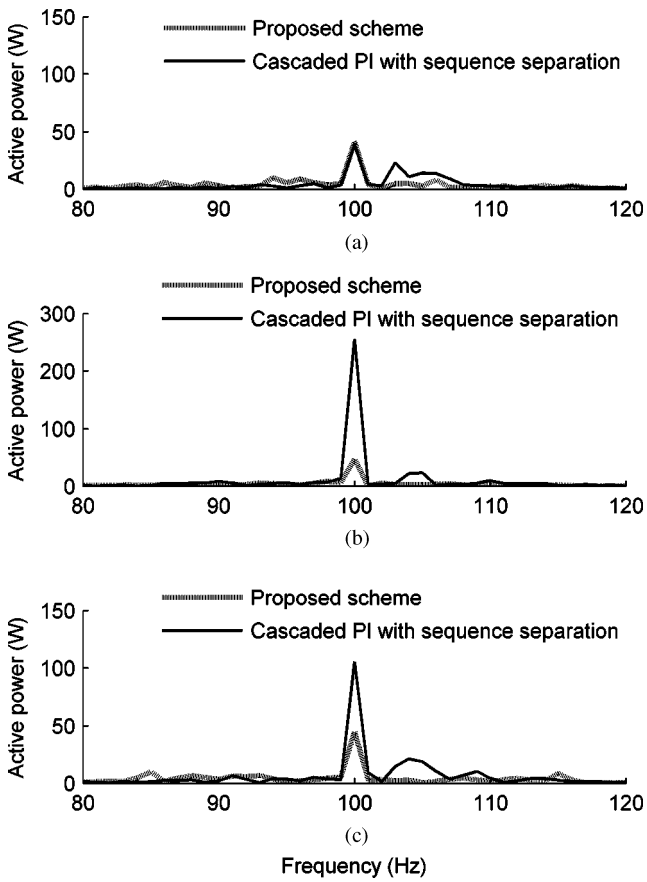

Fig. 13. Harmonic spectrum comparison of active power with active power ripple-minimized strategy when parametric error exists. (a) 1.0 L_m . (b) 0.5 L_m . (c) 1.5 L_m

reactive power satisfies (32), the terms periodic changing at twice the grid frequency in (24) and (25) equal to zero. Hence, the torque and reactive power have only zero-frequency components. Similarly, if (35) and (36) are satisfied, the periodic changing terms in (26) equal to zero, and hence, the active power ripples are eliminated.

Second, the experiment of the cascaded PI control scheme with positive- and negative-sequence separation, as proposed in [5], is also carried out. Both the positive-sequence and negative-sequence current loops are designed to obtain first-order closed-loop responses with 10 ms time constant. The torque/reactive power loop are designed to obtain first-order closed-loop responses with 50 ms time constant. Fig. 13 shows the active power harmonic spectrum with active power ripple-minimized strategy when the DFIG operates with a torque of –8 N·m and a reactive power of 1000 var. When the value of magnetizing inductance used in the controller equal to the actual machine parameter, the cascaded PI control scheme shows similar ripple-minimized effect with the proposed scheme, as shown in Fig. 13(a). To compare the parametric robustness, the value of magnetizing inductance used in the controller is set to $\pm 50\%$ departing from the actual value. Fig. 13(b) and (c) shows that the ripples are almost the same when the proposed ISM-DTC scheme is used, but increase when the cascaded PI control

scheme proposed in [5] is used. Hence, the proposed ISM-DTC scheme shows better parametric robustness.

IX. Conclusion

An ISM-DTC scheme with SVM is proposed to control the WECSs based on DFIGs under unbalanced grid voltage. Different control objectives can be achieved, including minimization of ripples in torque and stator reactive power, or minimization of ripples in stator active power.

Compared to existing control schemes of DFIGs under unbalanced grid voltage, the parametric uncertainties are included into the design procedure of sliding-mode controller, which guarantees the robustness of the system. Furthermore, because the torque and reactive power are directly controlled by rotor voltage, the measurement, coordinate transformation, and sequence decomposition of rotor current are eliminated, and the coordinate transformations of stator voltage and current are also eliminated, which simplifies the structure of the controller.

Simulation and experimental results verify that the proposed ISM-DTC scheme can effectively minimize the ripples in torque and power of the DFIG under unbalanced grid voltage, even if parametric errors exist.

Appendix

Machine Parameters

Stator rated voltage: 380 V.
Stator rated current: 4.5 A.
Rotor rated voltage: 120 V.
Rotor rated current: 10 A.
Operating frequency: 50 Hz.
Synchronous speed: 1500 r/min.
Magnetizing inductance (referred to the stator): 0.2987 H.
Rotor leakage inductance (referred to the stator): 0.0186 H.
Stator leakage inductance: 0.0186 H.
Rotor winding resistance (referred to the stator): 5.8985 Ω.
Stator winding resistance: 2.6596 Ω.
Stator-to-rotor turn ratio: 3.1667.

Acknowledgment

The authors gratefully acknowledge the contributions of K. F. Wong, W. W. Chan, and C. K. Cheung on the experimental setup or their technical support/advices.

References

[1] A. Petersson, T. Thiringer, L. Harnefors, and T. Petru, "Modeling and experimental verification of grid interaction of a DFIG wind turbine," *IEEE Trans. Energy Convers.*, vol. 20, no. 4, pp. 878–886, Dec. 2005.

[2] R. Pena, J. C. Clare, and G. M. Asher, "Doubly fed induction generator using back-to-back PWM converters and its application to variable-speed wind-energy generation," *Inst. Electr. Eng. Proc. Elect. Power Appl.*, vol. 143, no. 3, pp. 231–241, May 1996.

[3] E. Muljadi, D. Yildirim, and T. Batan, "Understanding the unbalanced-voltage problem in wind turbine generation," in *Proc. 1999 Int. Ind. Appl. Conf.*, pp. 1359–1365.

[4] T. A. Brekken and N. Mohan, "Control of a doubly fed induction wind generator under unbalanced grid voltage conditions," *IEEE Trans. Energy Convers.*, vol. 22, no. 1, pp. 129–135, Mar. 2007.

[5] L. Xu and Y. Wang, "Dynamic modeling and control of DFIG based wind turbines under unbalanced network conditions," *IEEE Trans. Power Syst.*, vol. 22, no. 1, pp. 314–323, Feb. 2007.

[6] J. B. Hu, Y. K. He, L. Xu, and B. W. Williams, "Improved control of DFIG systems during network unbalance using PI–R current regulators," *IEEE Trans. Ind. Electron.*, vol. 56, no. 2, pp. 439–451, Feb. 2009.

[7] Y. Zhou, P. Bauer, J. A. Ferreira, and J. Pierik, "Operation of grid-connected dfig under unbalanced grid voltage condition," *IEEE Trans. Energy Convers.*, vol. 24, no. 1, pp. 240–246, Mar. 2009.

[8] V. I. Utkin, J. Güldner, and J. X. Shi, *Sliding Mode Control in Electromechanical Systems*. Boca Raton, FL: CRC Press, 1999, pp. 115–130.

[9] L. Xu and P. Cartwright, "Direct active and reactive power control of DFIG for wind energy generation," *IEEE Trans. Energy Convers.*, vol. 21, no. 3, pp. 750–758, Sep. 2006.

[10] G. S. Buja and M. P. Kazmierkowski, "Direct torque control of PWM inverter-fed AC motors—A survey," *IEEE Trans. Ind. Electron.*, vol. 51, no. 4, pp. 744–757, Aug. 2004.

[11] D. Santos-Martin, J. L. Rodriguez-Amenedo, and S. Arnalte, "Direct power control applied to doubly fed induction generator under unbalanced grid voltage conditions," *IEEE Trans. Power Electron.*, vol. 23, no. 5, pp. 2328–2336, Sep. 2008.

[12] J. Holtz, "Pulsewidth modulation for electronic power conversion," *Proc. IEEE*, vol. 82, no. 8, pp. 1194–1214, Aug. 1994.

[13] S. K. Chung, J. H. Lee, J. W. Park, J. S. Ko, and M. J. Youn, "Current control of voltage-fed PWM inverter for AC machine drives using integral variable structure control," in *Proc. 1995 IEEE Ind. Electron., Control, Instrum. Conf.*, pp. 668–673.

[14] I. Munteanu, S. Bacha, A. Bratcu, J. Guiraud, and D. Roye, "Energy-reliability optimization of wind energy conversion systems by sliding mode control," *IEEE Trans. Energy Convers.*, vol. 23, no. 3, pp. 975–985, Sep. 2008.

[15] Z. Xu and M. F. Rahman, "Direct torque and flux regulation of an IPM synchronous motor drive using variable structure control approach," *IEEE Trans. Power Electron.*, vol. 22, no. 6, pp. 2487–2498, Nov. 2007.

[16] P. Albertos and A. Sala, *Multivariable Control Systems*. London, U.K.: Springer-Verlag, 2004, pp. 129–136.

[17] K. C. Wong, S. L. Ho, and K. W. E. Cheng, "Direct voltage control for grid synchronization of doubly-fed induction generators," *Electr. Power Compon. Syst.*, vol. 36, no. 9, pp. 960–976, Sep. 2008.

Si Zhe Chen was born in Shantou, China, in 1981. He received the B.Sc. degree in electromechanical engineering in 2005 from the South China University of Technology, Guangzhou, China, where he is currently working toward the Ph.D. degree with the College of Electric Power.

He is also a Research Assistant with the Department of Electrical Engineering, The Hong Kong Polytechnic University, Kowloon, Hong Kong. His research interests include the control and power electronics technology in renewable energy.

Norbert C. Cheung (S'85–M'91–SM'05) received the B.Sc. degree from the University of London, London, U.K., in 1981, the M.Sc. degree from the University of Hong Kong, Hong Kong, in 1987, and the Ph.D. degree from the University of New South Wales, Kensington, N.S.W., Australia, in 1995.

He is currently with the Department of Electrical Engineering, the Hong Kong Polytechnic University, Kowloon, Hong Kong. His current research interests include motion control, actuators design, and power electronic drives.

Ka Chung Wong was born in Hong Kong, 1981. He received the M.Eng.and the B.Eng. degrees in electrical engineering in 2004 from the Hong Kong Polytechnic University, Hong Kong, where he is currently working toward the Ph.D. degree.

He is currently a Tutor with the Hong Kong Polytechnic University. His research interests include control and drives for variable-speed power generation.

Jie Wu received the B.Sc. degree in automatic control from the Department of Electric Power, Harbin Institute of Technology, Harbin, China, in 1961.

He is currently a Professor and a Doctoral Supervisor with the College of Electric Power, South China University of Technology, Guangzhou, China. His current research interests include in the field of green energy sources and ecologic environment controls.